Journal of
Composites Science

MDPI

Article

A Study of the Interply Strengthening of CF/PA6 Composites Using Micro-Size Core-Shell Particles

Anurag Sharma * and Sunil Chandrakant Joshi *

School of Mechanical and Aerospace Engineering, Nanyang Technological University, 50 Nanyang Avenue, Singapore 639798, Singapore
* Correspondence: anurag006@e.ntu.edu.sg (A.S.); mscjoshi@ntu.edu.sg (S.C.J.)

Abstract: Thermoplastic composites have become increasingly popular due to their numerous benefits. To enhance the performance of fiber-reinforced thermoplastic composites, many research efforts have been made using various types of fillers. However, the high melting temperature and viscosity of thermoplastic polymer melt present a primary challenge in achieving uniform filler dispersion. Interply strengthening is one of the simplest and most cost-effective techniques for addressing this challenge. This study utilized micro-size core-shell particles that were dispersed using a sieve. The particles were carefully sprinkled onto the sieve, facilitating their controlled dispersion at the ply interface, after which fabric and thermoplastic films were laid on top. The resulting stacked arrangement was then processed using a hot consolidation cycle via compression molding to produce composite laminate. The impact of incorporating core-shell particles on the mechanical performance of carbon fiber-reinforced polyamide 6 (CF/PA6) laminates was investigated. Results showed that adding 4 wt% core-shell particles led to a maximum improvement of 58.99%, 25.62%, 41.56%, and 47.83% in flexural strength and modulus, interply shear strength, and compression strength, respectively, compared to the pristine composites. Stress-strain curves confirmed that the core-shell particles delayed matrix and interlaminar crack propagation. Furthermore, micrographic images indicated improved interaction of CSPs at the ply interfaces. These findings can improve the interply strength of thermoplastic composites and assist designers in achieving higher performance.

Keywords: interply strengthening; carbon fiber; thermoplastic composites; core-shell particles; flexural strength; ILSS; compression strength

Citation: Sharma, A.; Joshi, S.C. A Study of the Interply Strengthening of CF/PA6 Composites Using Micro-Size Core-Shell Particles. *J. Compos. Sci.* **2024**, *8*, 447. https://doi.org/10.3390/jcs8110447

Academic Editor: Steven Nutt

Received: 2 September 2024
Revised: 28 October 2024
Accepted: 29 October 2024
Published: 1 November 2024

1. Introduction

In recent decades, thermoplastic composites have gained widespread use due to their superior qualities, including exceptional durability, recyclability, unlimited shelf life, rapid production cycles, and other advantages over thermoset composites [1–4]. Carbon-fiber (CF) reinforced thermoplastic laminates are extensively used in aerospace, automotive, marine, and defense industries, where high specific strength and stiffness are crucial for various structural applications [1,5,6]. Throughout their operational lifespan, thermoplastic composites often encounter different loading conditions. Among the numerous failure mechanisms observed in thermoplastics, the most prevalent in woven composites are matrix cracks and interlaminar fracture, also known as delamination [7,8]. Notably, interlaminar fracture (delamination) poses a significant limitation to the use of composite laminates, as it leads to a substantial decrease in structural rigidity, often without visible signs of damage, potentially resulting in catastrophic failure [9–11]. Consequently, there is a need to understand underlying issues and find ways to enhance performance. This work investigates the use of micro-particles to bring about interply strengthening in the laminates, thereby enhancing the mechanical performance of thermoplastic composites.

Various researchers have proposed different methods, such as filler reinforcement and sizing of fiber for better fiber/matrix interaction, to improve mechanical performance and

enhance the interply strength of thermoplastic composites [12–14]. In efforts to enhance the interfacial interaction between fiber and matrix, numerous researchers have explored the use of chemical modification and specific treatment for the fiber sizing [15–20]. Nassehi et al. [21,22] investigated the modification of fibers through sizing, which served as the interphase between the fibers and the matrix, thereby improving the mechanical performance of resulting composites. Specifically, a ductile thermoplastic sizing with a modulus ranging from 5 GPa to 1 GPa performed better than rubber-based sizing (modulus ~10 MPa) on the fibers, as it promoted a more uniform stress distribution between the fiber and the matrix. In recent advancements, Yan et al. [15] employed a polyamide-based sizing agent to improve the wettability of the carbon fibers, which facilitated better resin impregnation at the fiber surface in carbon fiber reinforced polyamide 6 (CF/PA6) composites. This approach resulted in a 14.2% increase in interlaminar shear strength (ILSS) and a 20% improvement in flexural strength, as the sizing agent acted as a stress-transfer bridge between the fibers and the matrix. Similarly, Gocke et al. [16] utilized electrochemical oxidation treatment to enhance the interfacial adhesion of CF/PA6 composites, achieving an 11.7% increase in flexural strength by creating a mechanical interlock between the fiber surface and the matrix. Recently, a comprehensive review by Zheng et al. [23] summarized various techniques for modifying fiber interface to improve the surface activity [24,25], roughness [26,27], and wettability [28], thereby enhancing interfacial adhesion between fiber-matrix and mechanical properties. However, modifying fiber sizing is a specialized task and may involve high cost and difficulties in scaling up for large-scale production [29–31]. Therefore, this current study is focused on using fabric and thermoplastic matrix as received from the manufacturer.

On the other hand, another approach involves incorporating reinforcing fillers within the polymer matrix, or at the ply interfaces and fabric interstices, referred to as interply strengthening. For reinforcement in thermoplastic polymer matrices, Shen et al. [32] noted that 2 wt% reinforcement of carbon nanotubes in glass fiber/PA6 laminates led to a 36% increase in flexural performance. This improvement was primarily due to enhanced interfacial interaction between fiber/matrix. Additionally, Chen et al. [33] modified thermoplastic composites by incorporating silica particles which resulted in a 15% improvement in ILSS and a 13.9% enhancement in flexural strength. They attributed this enhancement to the filler's ability to hinder matrix crack initiation and propagation. Qiao et al. [34] and Su et al. [35] examined how carbon nanotubes enhance the mechanical performance of CF-PEEK laminates. They used solvent evaporation and ultrasonic mixing to distribute the fillers, resulting in improved performance due to better fiber-matrix interaction. However, challenges in dispersing fillers in thermoplastics using these techniques are attributed to the requirement of high-temperature mixing conditions with the high viscosity of polymer melt, which restricts uniform dispersion and leads to undesirable agglomeration [36–38].

To overcome the challenges faced in fiber sizing and filler dispersion, the interlaminar filler reinforcement technique, also known as interply strengthening, has emerged as a more practical and cost-effective approach for filler dispersion in thermoplastic polymers [39]. While this method has proven effective for thermoset composites, its application in thermoplastic composites remains limited [12,40,41]. A comprehensive literature review by Sharma and Joshi [7] identified micro-sized core-shell particles (CSPs), consisting of a poly(butyl acrylate) rubbery core and a poly(methyl methacrylate) polymer shell, as the most effective filler for interfacial dispersion due to their cost-effectiveness, ease of dispersion, chemical compatibility with the polyamides, epoxies, and polyesters, and significant improvement in mechanical properties as compared to silica, alumina, carbon nanotubes, and graphene oxides. In a recent study, Sharma and Joshi [42] examined the impact of CSPs on the fatigue performance of thermoplastic laminates. The investigation revealed that the fatigue life was increased by eight-fold. A possible reason behind the improvement was the interaction between functionalized group on PMMA shell and PA6 matrix, which promoted adhesion at the ply interface and delayed failure. The CSPs remain discrete without agglomerating, promoting their uniform distribution [41,43]. The unique core-shell structure integrates

a rubbery core and glassy shell system, which contributes to the failure mechanism in composites. The core functions to absorb energy, while the shell undergoes melting to bond with the matrix and fiber or with interfaces [44,45]. Despite extensive research on CSPs as reinforcing agents in thermoset composites, their application and behavior in thermoplastic composites remain understudied. This current study on enhancing interply strength of thermoplastic composites using micro-sized CSPs presents a novel technique for improving mechanical performance in an easy and cost-effective manner, having potential for large scale production.

This study involves reinforcing woven carbon fiber in a PA6 matrix to fabricate composites, with varying amounts of CSPs dispersed at the ply interfaces, specifically 2 wt%, 4 wt%, and 6 wt%. A uniform distribution was achieved through manual dispersion assisted by sieving. To evaluate the effect of CSPs on interply strengthening and their overall contribution, three-point bend tests, short beam tests, and compression tests were performed. Furthermore, potential contributing failure mechanisms were identified and examined. Microscopic analysis was conducted to examine various failure mechanisms/modes associated with the mechanical characteristics.

2. Materials and Methods

2.1. Materials

The two-by-two twill CF (HexForce 48302 WE1270) weave fabric was supplied by Hexcel Corporation USA, utilizing IM2C-12K grade CF tows. The fabric has an areal density of 300 g/m^2 and features a balanced tow construction with a yarn density of 3.35 yarn/cm in both the wrap and weft direction. The polymer matrix, a 0.5 mm thick PA6 (Sustamid-6) film, was procured from the Röchling Group, Germany (melting point of 220 °C). All mechanical properties of CF fabric and PA6 are tabulated in Table 1. The grade of CSPs was Paraloid EXL-2314 and they were supplied by Dow Chemical Pacific (Singapore) Private Limited, featuring a core-shell architecture with a rubbery cross-linked poly–butyl–acrylate (PBA) core and a glassy poly (methyl methacrylate) (PMMA) shell as shown in Figure 1. Notably, the PMMA shell is functionalized with glycidyl methacrylate (GMA) groups, which facilitate reactions with polyamides, and epoxies resins. The reaction mechanism involves the amine group in polyamides reacting with the epoxy ring of GMA, forming covalent bonds that improve compatibility within the blend. The particles have an overall micro-size of 550 nm with a core-to-shell weight ratio of 20 to 80%, as specified by the supplier.

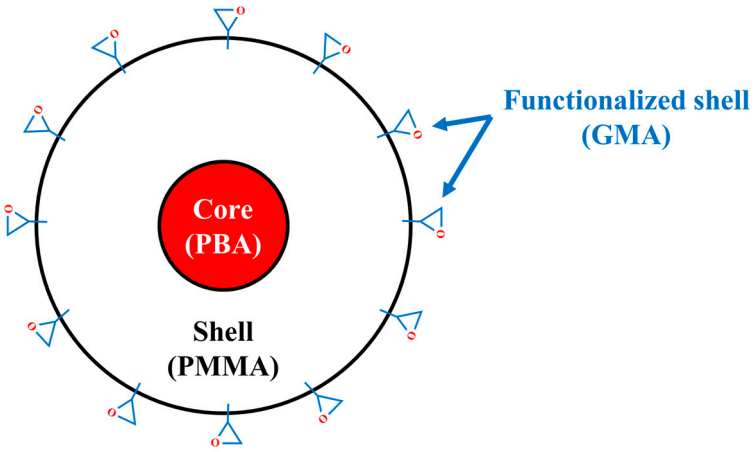

Figure 1. Architecture of core-shell particles.

Table 1. Mechanical characteristics of CF fabric and PA6.

Materials	Tensile Strength (MPa)	Young's Modulus (GPa)	Density (g/cm^3)	Thickness (mm)
CF fabric	5723	296	1.78	0.5
PA6	80 (yield)	3.2	1.14	0.5

2.2. Composites Manufacturing

The manufacturing of CF/PA6 composites was completed through hot compression molding, with the process detailed in Figure 2a–f.

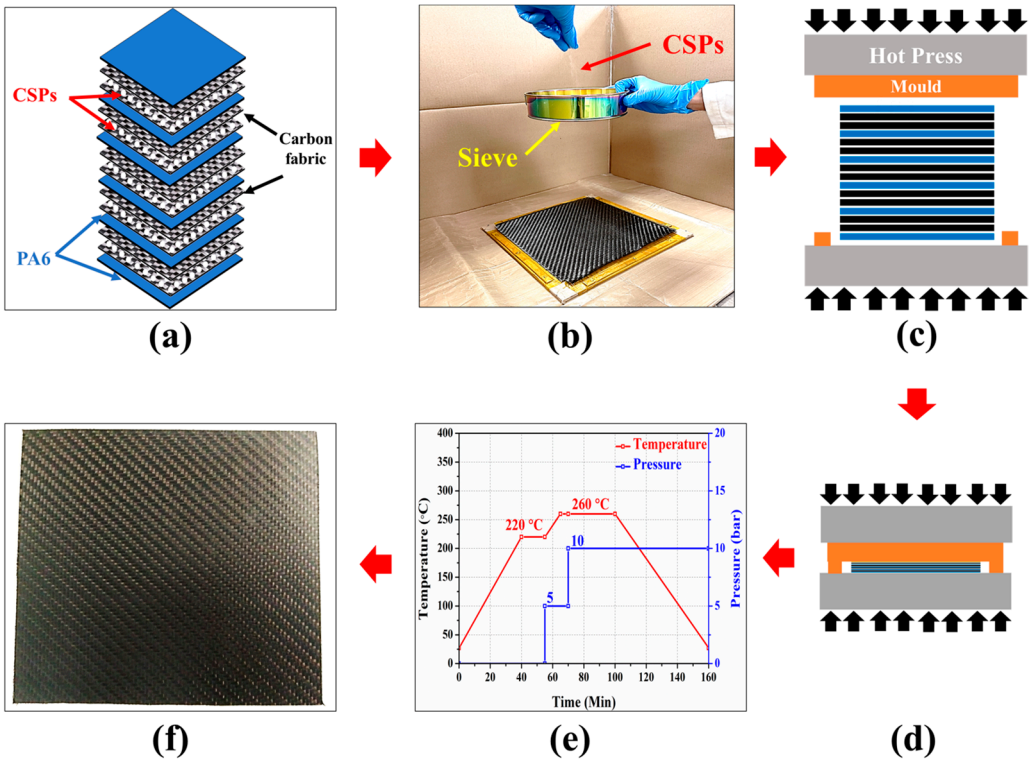

Figure 2. Manufacturing Process for CF/PA6 composites; (**a**) CSPs dispersed at the ply interfaces; (**b**) Manual dispersion of filler using a sieve; (**c**,**d**) Hot press compression molding; (**e**) Two-step consolidation cycle; (**f**) Manufactured composites.

Initially, the lay-up sequence was designed in which 10 layers of CF fabric, each measuring 28 cm × 28 cm, were alternated with 6 films of PA6, each measuring 25 cm × 25 cm and weighing 35.62 g, in a specific sequence. The strategic positioning of the polymer films and fabric was optimized to ensure uniform distribution of the matrix throughout the fiber network for high-quality composites (refer to Figure 2a). During the layup process, 8.54 g of CSPs, equivalent to 4 wt% of the polymer mass, were dispersed using a sieve (refer Figure 2a) and distributed evenly across all five CF ply interfaces, with 1.70 g applied per ply interface. The particles were carefully sprinkled onto the sieve, facilitating their controlled deposition at the ply interface and fabric interstices (refer to Figure 2b). The dispersion process was assisted by a sieve with a mesh size of 180 µm to prevent agglomeration issues and achieve uniform spread of CSPs on the CF fabric. The quality of dispersion was visually examined, as depicted in Figure 3a,b, which showed the dispersion of filler on the ply interface and fabric interstices for 2 wt% compared to pristine.

Subsequently, the stacked layup was placed onto a 3 mm thick aluminum 6061 mold and consolidated using a carver hydraulic hot press. The two-step consolidation cycle used is presented in Figure 2e. During the consolidation phase, two possible scenarios

occurred. In the first scenario, the CSPs remained at the ply interfaces. In the second scenario, the PMMA shell of CSPs melted and exposed the inside nanoscale PBA core. This core can permeate the fiber bundle and blend with the matrix at the fiber interstices. Finally, manufactured composites were sectioned using a rotating saw to prepare specimens for various testing. The other composites were also manufactured in the same way. The average thickness of 0, 2, 4, and 6 wt% were 3.25 ± 0.04 mm, 3.33 ± 0.03 mm, 3.42 ± 0.05 mm, and 3.51 ± 0.09 mm, respectively. The observed increase in thickness was primarily attributed to the increased number of particles dispersed at the ply interfaces, which contributed to the overall thickness of the composites.

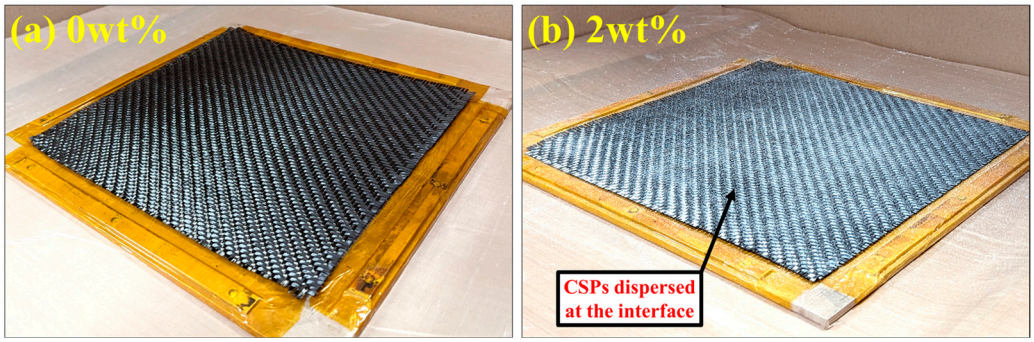

Figure 3. Interface of carbon fabric for (**a**) pristine and (**b**) 2 wt% CSPs modified CF/PA6 composites.

2.3. Test Methods

2.3.1. Bending Test

The three-point bend test was carried out following ASTM D7264 [46] standard for the flexural specimens, which had a span length-to-thickness (L/t) ratio of 32, as illustrated in Figure 4. The test was conducted using an Instron testing equipment coupled with a 50 kN load cell and a crosshead speed of 1 mm/min. The samples were produced following ASTM standard, and the dimensions of the samples were (115 × 13 × 3) mm. Instron 5569 Blue-hill software (version 4.01) was used to control the test and analyze the collected data. This test was performed to determine the flexural performance values such as stiffness and strength of composites.

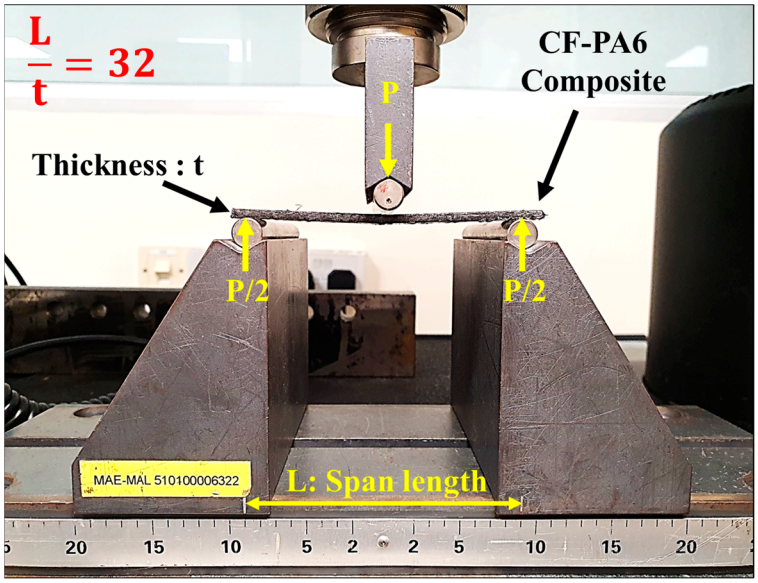

Figure 4. Three-point bending test fixture and loading diagram of the samples tested.

2.3.2. Short Beam Shear Test

The short beam shear (SBS) tests were conducted following ASTM D2344 [47] to determine ILSS and the fixture used is shown in Figure 5a. The tests were conducted using a Shimatzu machine (autograph AG-X series) with a crosshead speed of 1.0 mm/min with a load cell capacity of 10 kN. Six samples were tested for all the composites. The samples were produced following ASTM standard, and the dimensions of samples were 18 mm × 6 mm × 3 mm. The ILSS was calculated using the formula suggested by standard in which maximum load within the elastic limit, sample width, and thickness were used.

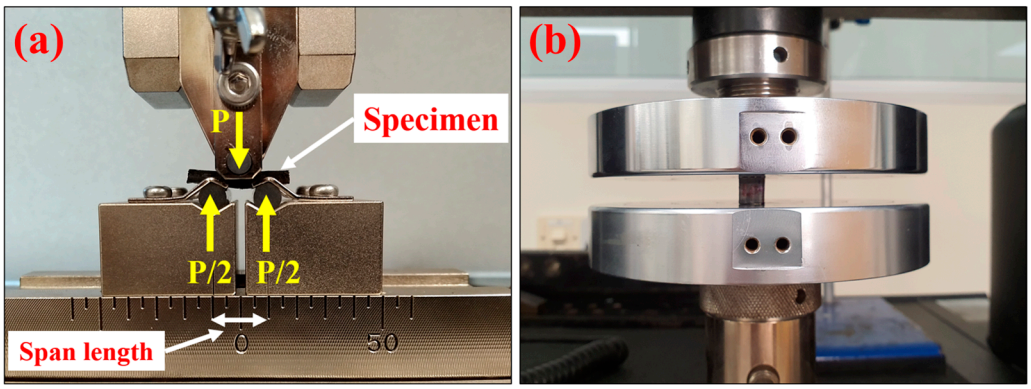

Figure 5. (**a**) Short-beam shear test fixture (**b**) compression loading of the samples.

2.3.3. Compression Strength

The compressive performance of the CF/PA6 laminates was assessed following ASTM D695 [48] test fixture as depicted in Figure 5b. The objective of this test was to evaluate the deformation characteristics of laminates under compressive load until significant failure occurred. The test was performed using Instron testing equipment with a capacity of 50 kN load and a crosshead speed of 1.3 mm/min. The samples were prepared according to ASTM standard with dimensions of (10 × 10 × 3) mm. The compressive strength and compression modulus of laminates were determined using load and deformation data obtained from the test.

2.3.4. Interfacial Observations

To obtain more in-depth knowledge about failure modes, microscopic examinations were conducted on the damaged samples using an Olympus, Tokyo, Japan, optical microscope (SZX7 model). Furthermore, a thorough analysis of the CSPs interaction with the fiber and matrix was performed using a JEOL Tokyo, Japan scanning electron microscope (JSM-5500LV model).

3. Results and Discussions

3.1. Quality of Manufactured Composites

The quality of the manufactured laminates was assessed by evaluating the fiber volume content (V_f) and void volume content (V_c). To begin with the fiber volume content, Ignatius et al. [49] proposed a method for woven composites that utilizes known mass and volume properties of the matrix and fabric. The suggested equation for calculating the fiber volume fraction is as follows:

$$\text{Fiber volume content} : V_f = 1 - \frac{M_c - M_f}{d_m \times A \times t_c} \quad (1)$$

where M_c—mass of composites, M_f—mass of fibers, A—area of composites, d_m—density of matrix, t_c—thickness of composites.

Figure 6 illustrates the trend of the determined values concerning CSP content in weight percent. The trend showed that the fiber volume content decreased from 56.33 ± 1.40% for

pristine composites to 52.44 ± 2.12% for composites containing 6 wt% CSPs, illustrating that the incorporation of CSPs led to the replacement of polymer matrix, ultimately reducing the fiber volume content. The results were further corroborated by determining the void volume content (V_c). In pristine composites, the high viscosity of PA6 during the hot press consolidation process (low shear rate) reduced its flow, potentially leading to void formation within the composites. The V_c was determined using Equation (2), as suggested in ASTM D2734 [50] standard:

$$\text{Void volume content} : V_c(\%) = 100 - d_c\left[\frac{\%M_m}{d_m} + \frac{\%M_f}{d_f}\right] \quad (2)$$

Here, $\%M_m$—mass percentage of matrix, $\%M_f$—mass percentage of fiber, d_m—density of composite.

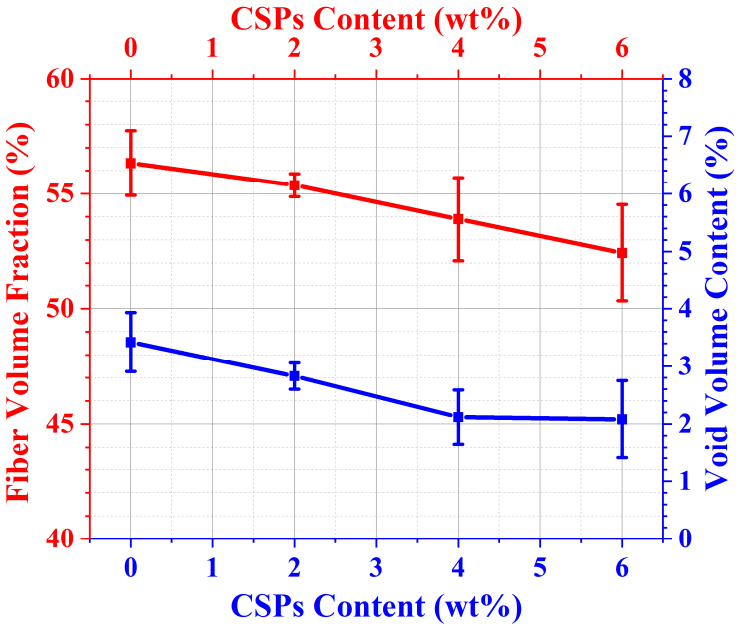

Figure 6. Fiber volume content and void volume content of composites modified with CSPs.

The results indicated that the void volume content decreased from 3.42 ± 0.51% for pristine composites to 2.08 ± 0.67% as the particle content increased up to 6 wt%. This suggests that the dispersion of CSPs is crucial for reducing void volume content. The reduction in void volume content was facilitated by the melting of PMMA shell and its subsequent adhesion to the matrix. At the lower CSPs content, the PMMA remained at the ply interface, and the functionalized GMA group on the PMMA improved interfacial adhesion to the PA6 matrix, thereby improving the overall quality of the composites. The void volume content values confirm the high quality of the manufactured composites, as they remained around 2–3%, which is within the range recommended by several researchers [51].

3.2. Flexural Characteristics

Three-point bend tests were performed to determine the flexural strength and modulus of CF/PA6 laminates modified with CSPs. The impact of varying CSPs content on the flexural performance of the laminates was examined and compared with the original composites. Figure 7a illustrates the characteristic stress versus strain curve for the composites and the effects of CSPs on the prepared composites. In Figure 7a, none of the specimens experienced a sharp fracture, indicating that the failure was primarily due to matrix cracking and minor delamination. Figure 7a also demonstrates that the 2 wt% and 4 wt% CSP-modified composites experienced delayed failure occurrence, as indicated by the delayed maximum stress peak compared to the pristine composites. However, for

the 6 wt% CSPs modified composites, the stress peak was similar to that of the pristine sample. This can be attributed to the higher concentration of CSPs at the ply interfaces, which increased cohesion between particles, thereby promoting faster crack propagation and reducing flexural strength. Furthermore, the non-uniform CSPs distribution at the ply interfaces likely contributed to premature failure in the composites.

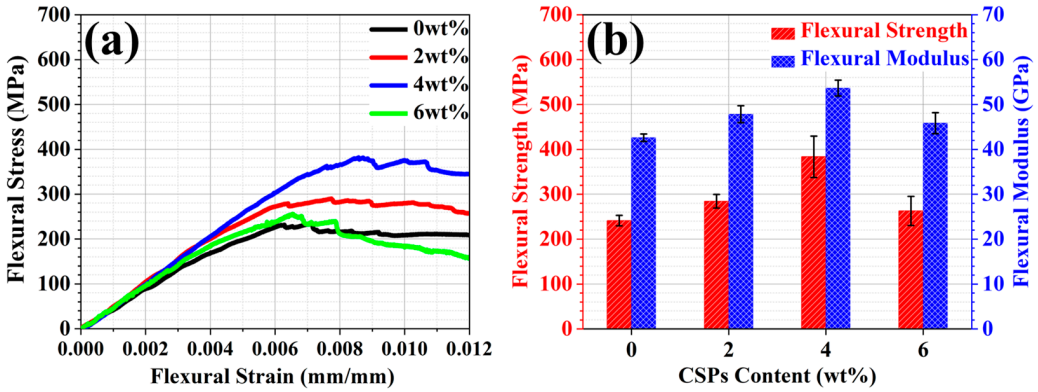

Figure 7. Influence of CSPs on flexural performance of CF/PA6 laminates, showing (**a**) Flexural stress versus flexural strain curves (**b**) a bar chart comparison between strength and modulus.

For comparison, Figure 7b presents a bar chart that includes the average flexural strength, modulus, and associated deviation for all composites. Incorporating 4 wt% CSPs to CF/PA6 laminates led to a significant increase in flexural strength from 241.18 ± 11.67 MPa in the 0 wt% composites to 383.47 ± 46.19 MPa, signifying a 58.99% enhancement. When evaluating these outcomes in the form of efficiency factors, considering both strength ($\mu_{strength}$) and modulus ($\mu_{modulus}$) (refer to Equations (3) and (4)), higher efficiency factor values indicate greater strength or modulus per unit particle content. An optimal performance was achieved when these factors were maximized, indicating that a minimal amount of filler could yield the maximum strength. As shown in Table 2, the laminates with 4 wt% CSPs demonstrated the maximum strength per unit CSPs content. The increases in flexural strength could be attributed to the interaction between the functionalized shell of the CSPs and the PA6 matrix, which can lead to the formation of covalent bonds that significantly enhance interfacial interaction and adhesion. However, increasing CSPs content to 6 wt% resulted in a significant decrease in flexural performance compared to the 4 wt% composites. The reduction in strength was primarily due to the increased interfacial thickness. The higher CSP content at the ply interface may cause to form relatively large domains of CSPs, thereby increasing ply interface thickness. This promoted premature crack initiation and propagation in the 6 wt% composites, ultimately leading to reduced strength. Additionally, the non-uniform distribution of CSPs at the 6 wt% caused inconsistencies at the ply interface, contributing to a premature failure of the composites under flexural load. Regarding the modulus, the observed decrease in modulus of 6 wt% composites can be attributed to the increased exposure of the PBA core, which has a much lower Young's modulus compared to PA6 matrix.

$$\mu_{strength} = \frac{\text{Flexural Strength}_{CSPs} - \text{Flexural Strength}_{pristine}}{\text{CSPs content (wt\%)}} \quad (3)$$

$$\mu_{modulus} = \frac{\text{Flexural Modulus}_{CSPs} - \text{Flexural Modulus}_{pristine}}{\text{CSPs content (wt\%)}} \quad (4)$$

Table 2. Flexural efficiency factors for pristine and CSPs modified CF/PA6 laminates.

CSPs Content (wt%)	Strength Efficiency Factor (MPa/wt%)	Modulus Efficiency Factor (GPa/wt%)
0	-	-
2	21.59	2.62
4	35.57	2.76
6	3.62	0.54

Figure 8a–d displays microscopic images of the center region of the side cross-section for all composite specimens. The fractured surfaces exhibit fiber breakage, fiber bundle buckling, and fiber bundle delamination. These observations were utilized to determine the failure mechanisms of the composites during flexural loading. In pristine composites, the failure mechanism begins with matrix cracks originating from a fiber bundle before any deflection at the knee point. Subsequently, cracks spread and accumulate progressively within the fiber bundles. At high stress levels, intralaminar cracks (cracks between fiber bundles) emerge, leading to a noticeable decrease in stiffness, as evidenced by the slope change in the flexural stress–strain relationship (see Figure 7a). After the peak point, fiber bundle debonding occurs, while fiber bundle buckling and debonding are only observed as flexural deflection increases near ultimate damage. The optical micrographs clearly show that fiber breakage, interlaminar cracks, fiber bundle buckling, and delamination are common failure modes resulting in final damage, similarly to the observations made by Ma et al. [52] and Zhao et al. [53]. This suggests that the decrease in flexural strength is primarily attributed to intralaminar and interlaminar cracks, fiber bundle debonding and buckling, and complete delamination of laminas in the case of pristine composites.

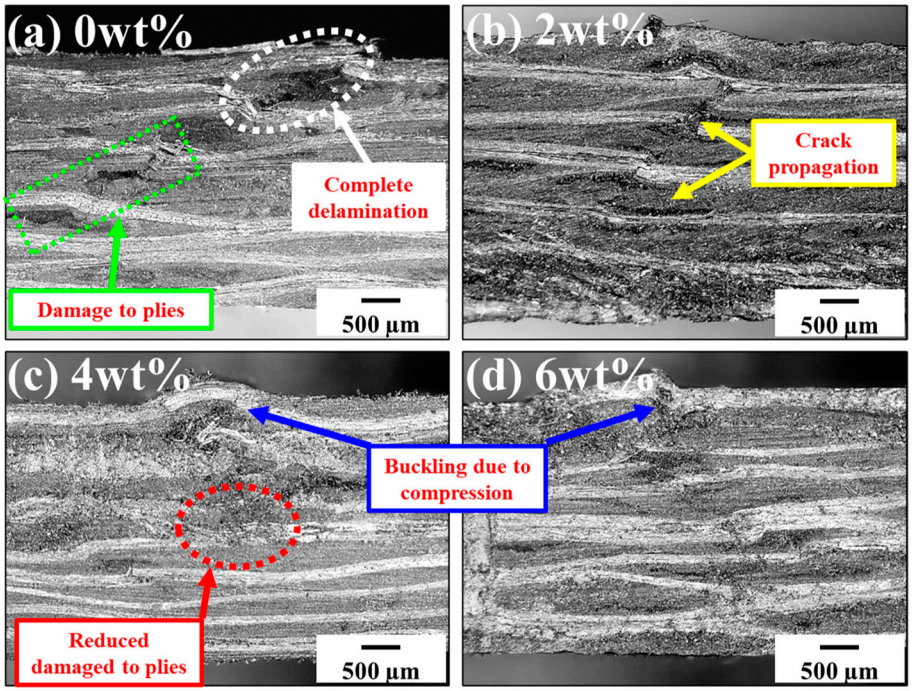

Figure 8. Microscopic image of the side cross section (center region) of flexural samples and their fractured surfaces for (**a**) 0 wt% (**b**) 2 wt% (**c**) 4 wt% (**d**) 6 wt% CSPs modified composites.

The reinforcement of CSPs into CF/PA6 laminates led to comparable behavior across 2, 4, and 6 wt% samples, except for the delay in failure and improvement in flexural strength. Figure 8c clearly demonstrates reduced ply damage in 4 wt% composites compared to Figure 8a for pristine composites. When CSPs were incorporated within the matrix, either embedded in the fabric tows or exposed PBA core, they acted as a hindrance to crack

initiation and growth, thereby significantly delaying the failure. When CSPs were located at the ply interfaces, they facilitated bonding between fabric layers. The dispersion of CSPs at fabric interfaces and within the matrix is evident in the SEM images depicted in Figure 9a,b. Notably, Figure 9c verifies the CSPs morphology observed through the optical microscope. As crack density reached its maximum, the delamination commenced in the composites. However, in CSPs modified composites, the availability of CSPs at ply interfaces strengthened the bonding between fiber bundles, resulting in improved flexural strength compared to unmodified composites.

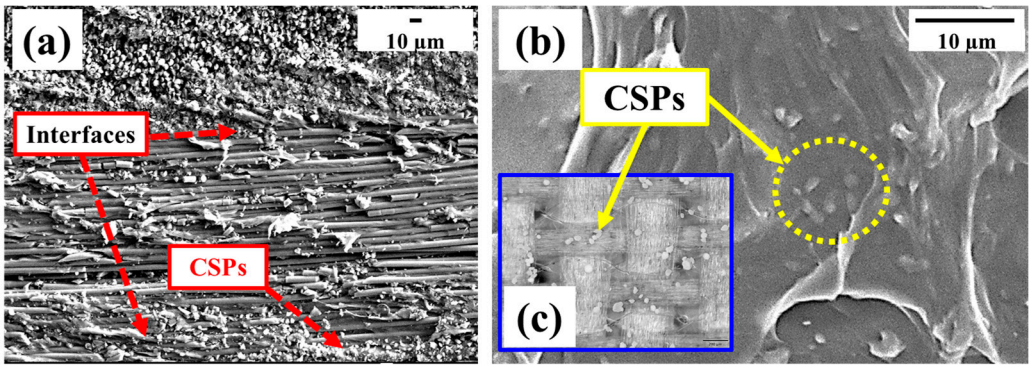

Figure 9. SEM micrograph of the side cross section (center region) of specimens, showing dispersion and presence of CSPs at (**a**) ply interfaces and (**b**) embedded within the matrix; (**c**) a separate optical micrograph illustrating CSPs morphology.

3.3. Interlaminar Characteristics

To evaluate the ply integrity and measure the interply strength of the CF/PA6 composite, the SBS test was performed. The SBS test involved applying load to an overhang sample with a very short gage length. Consequently, the crack propagated in the axial direction while also experiencing bending, indicating that crack propagation did not occur solely in the axial direction. This scenario presented the possibility of three failure modes: shear and inelastic deformation. Shear failure occurs when delamination between laminas is followed by matrix crack propagation in fiber bundles. The initiation of matrix cracks may be attributed to voids and defects within the matrix, which become areas of maximum stress concentration.

Figure 10a depicts the force versus deflection curve for all the composites. The maximum ILSS of the laminates is determined by the peak load it can bear along the axial direction. After reaching this peak, continued load application results in plastic deformation and fiber compaction, altering the specimen's geometry. Consequently, a maximum deflection of 0.60 mm was chosen to calculate ILSS. As shown in Figure 10b, the average ILSS values for CSPs content of 0, 2, 4, and 6 wt% were 24.66 $\pm$ 2.08 MPa, 31.91 $\pm$ 1.21 MPa, 34.91 $\pm$ 4.44 MPa, and 29.12 $\pm$ 2.42 MPa, respectively. The most significant improvement was noted in the 4 wt% composites, which demonstrated a 41.56% increase in ILSS. This improvement can be due to the high-quality laminate with minimal void volume content at higher concentrations of CSPs, as well as the excellent compatibility between particles, matrix, and fibers. As previously mentioned in the flexural properties section, the interaction between CSPs and fiber surfaces creates strong interfacial adhesion, leading to mechanical interlocking and improved shear properties. However, when CSPs content increased to 6 wt%, the greater amount of PMMA shell available at the ply interface may lead to more pronounced cohesion between particles, forming a relatively large domain of CSPs, thereby increasing ply interface thickness. This promoted faster crack propagation at the ply interface and ultimately reduction in ILSS. Additionally, the non-uniform distribution of CSPs at higher concentrations caused inconsistencies at the ply interface, contributing to the premature failure of the composite under shear loading.

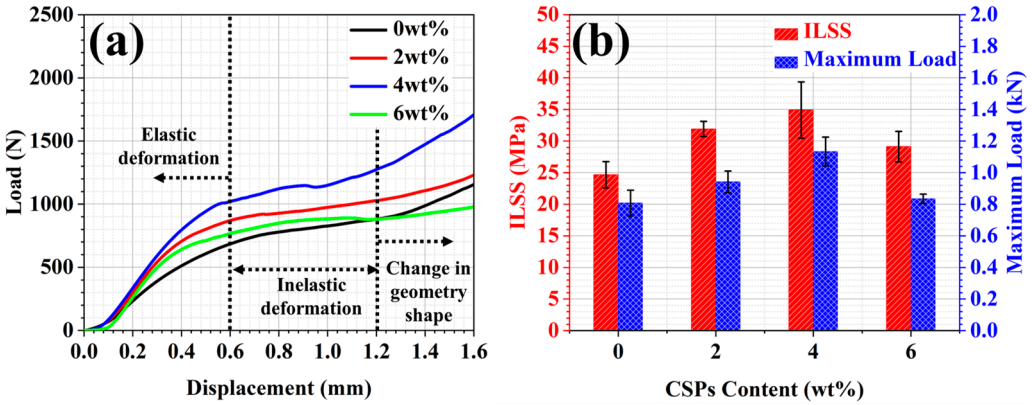

Figure 10. Role of CSPs in CF/PA6 laminates, showing (**a**) load versus displacement curves; (**b**) a bar chart comparison between ILSS and maximum load.

The failure modes and mechanisms were investigated through microscopic examination of the cross-sectional view, which revealed interlaminar shear cracks and deformation failures, as depicted in Figure 11a–d. The initial occurrence of interlaminar shear cracks during testing was attributed to pre-existing cracks within the matrix and at interfaces. The incorporation of CSPs at the ply interfaces significantly delayed the failure process by enhancing adhesion between the fiber layers, thereby mitigating slippage between the laminas. As shown in Figure 11a, the pristine composites exhibited complete delamination, in contrast to the behavior observed in Figure 11c for 4 wt% composites. As the load increases, this interaction may break and lead to inelastic deformation of the composites. As the strain further increases, the load can compact some of the fiber bundles changing the geometric shape, which in turn leads to a sudden increase in the load. The presence of interlaminar shear cracks in pristine, CSPs presence at the ply interfaces, and inelastic deformation were highlighted by the microscopic evidence shown in Figure 11c,d.

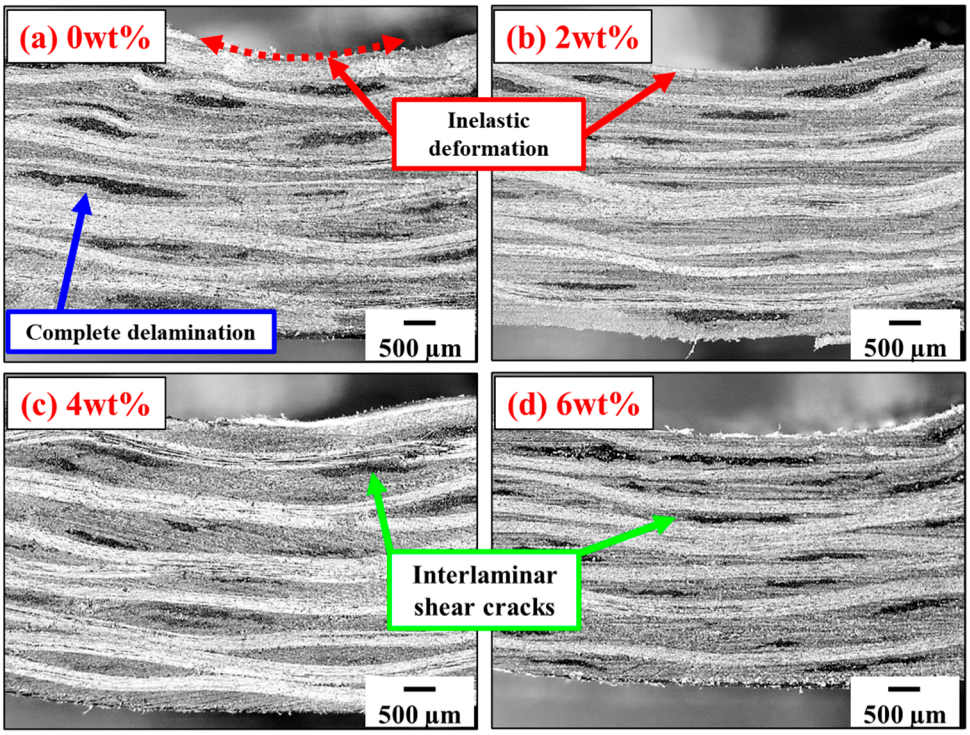

Figure 11. Side cross section (center region) of short beam test samples and identified failure modes using microscope for (**a**) 0 wt%; (**b**) 2 wt%; (**c**) 4 wt%; and (**d**) 6 wt% CSPs modified composites.

3.4. Compression Characteristics

The influence of CSPs on the compressive properties was assessed and compared to composites without CSPs (0 wt%). Figure 12a illustrates the compressive stress-strain curves for pristine and CSP modified CF/PA6 laminates. Notably, the compressive load rises linearly with displacement. The maximum stress point provided the compression strength, while the slope of elastic region provided the compression modulus. As the compression plate moved down, the material reached its yield point, and a sudden load drop was observed. This behavior suggests that the composites experienced multiple-ply cracking, fiber bundle buckling, crushing, and delamination. The incorporation of CSPs led to improvements in both compressive strength and modulus, as summarized in Figure 12b. Specifically, adding 4 wt% particles to the CF/PA6 laminates led to a significant enhancement in compressive strength and modulus, rising from 60.29 ± 5.68 MPa in the pristine composites to 83.12 ± 2.94 MPa, reflecting a 47.83% improvement. However, further increasing the CSP content to 6 wt% resulted in lower compressive strength and modulus due to significant cohesive interaction among the particles at the ply interface, forming a relatively large domain at the ply interface, which led to faster crack propagation.

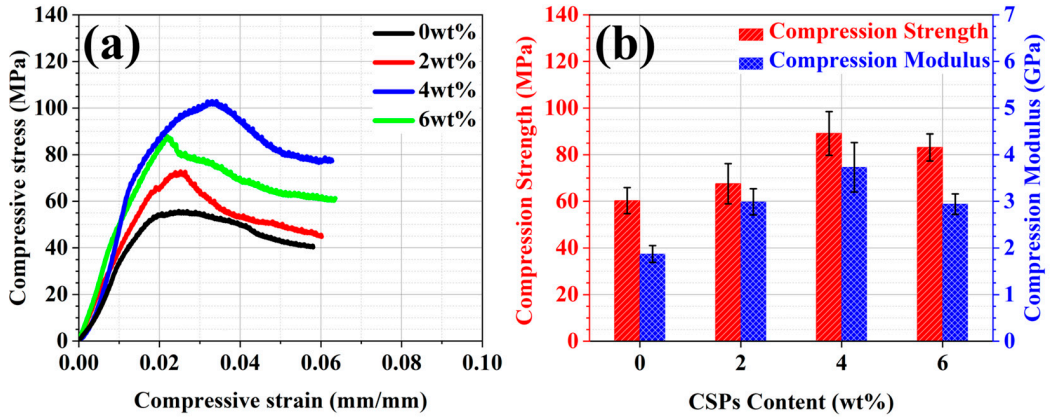

Figure 12. Impact of CSPs on CF/PA6 laminates, showing (**a**) compressive stress versus strain curves; (**b**) a bar chart comparison between strength and modulus.

For all the compression test specimens, the side cross-section was examined under an optical microscope. Notably, the upper section of the specimens was in contact with the top compression plate. Micrographic analysis of the failed samples revealed that the specimen's top surface was majorly damaged as compared to the bottom side, which was consistent with the observed failure location. The fracture surface of the failed specimens exhibited typical fracture features of composite materials, including ply cracking, and crushing, buckling of fibers, and delamination as shown in Figure 13a–d. In Figure 13a for pristine composites, the laminas went under extensive damage, whereas CSPs modified composites showed a sign of delays in the failure process (refer to Figure 13b,c).

Overall, the results presented in Figures 12 and 13 demonstrated that the reinforcement of CSPs controlled the damage in CF/PA6 laminates by enhancing interply strength and delaying crack propagation. The observed failure modes were corroborated by the analyses of flexural, ILSS, and compression characteristics. These findings suggest a significant potential for CSPs to reinforce the interfacial regions in thermoplastic composites, thereby improving their mechanical performance.

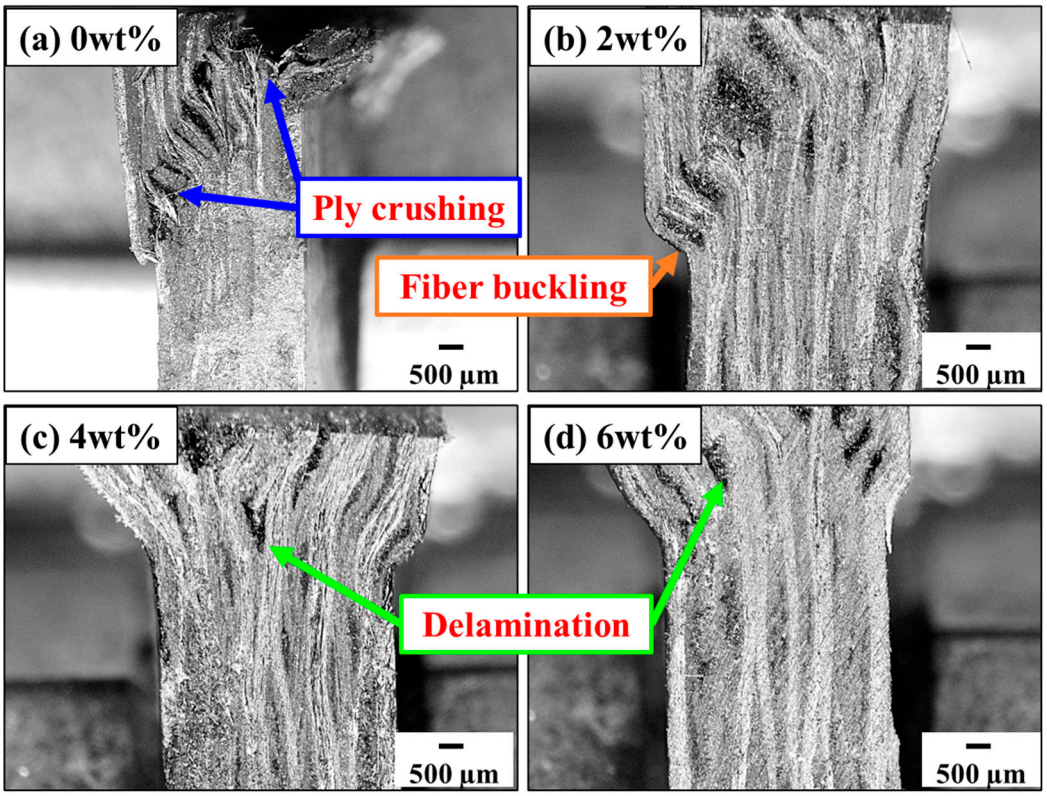

Figure 13. Side cross section (upper section) of compression samples and identified damage modes using the microscope for (**a**) 0 wt%; (**b**) 2 wt%; (**c**) 4 wt%; and (**d**) 6 wt% CSPs modified composites.

4. Conclusions

In this study, the CF-PA6 composites modified at their ply interfaces and fabric interstices using CSP fillers were tested under flexure, ILSS, and compression. The CSPs content varied from 2 wt% to 6 wt%. The CSP-modified composites reached the maximum strength and modulus values when the CSPs content was 4 wt%. The reinforcement of 4 wt% CSPs led to a maximum improvement in flexural strength, from 241.18 ± 11.67 MPa for the pristine composites to 383.47 ± 46.19 MPa, representing an improvement of 58.99%. Furthermore, the optimal improvement of 41.56% in ILSS was found at 4 wt%, compared to the pristine composites. Similarly, the compressive strength improved by 47.83%. Notably, an increase in CSPs content to 6 wt% led to a significant reduction in these mechanical properties. The higher CSPs content at the ply interface could be attributable to the formation of relatively large domains of CSPs due to cohesion between particles, which could have promoted faster crack propagation in the composites. The possible mechanisms of CSPs in CF/PA6 laminates were identified and discussed based on observed fractured specimens. It was evident that pristine composites underwent significant damage compared to those observed in CSPs composites. This implies that the incorporation of CSPs in the polymer matrix, whether embedded in the fabric tows or as fully melted CSPs with an internal PBA core, served as a hindrance to crack initiation and growth, significantly delayed failure. Additionally, CSPs located at the ply interfaces enhanced bonding between fabric layers, ultimately increasing interply strength and further delaying failure. Thus, CSPs exhibited a positive effect and improved the mechanical performance of thermoplastic composites through their unique interaction with fiber and matrix. These findings suggest that the interply toughening method is an effective approach for enhancing the mechanical performance of thermoplastics structures. By addressing challenges related to dispersion quality, this method presents a promising solution for practical applications across various industries. To facilitate industrial scalability, further exploration of advanced dispersion techniques, such as automated and pump-assisted techniques, is recommended.

Author Contributions: Conceptualization, A.S. and S.C.J.; methodology, A.S.; software, A.S.; validation, A.S. and S.C.J.; formal analysis, A.S.; investigation, A.S.; resources, S.C.J.; data curation, A.S.; writing—original draft preparation, A.S.; writing—review and editing, A.S. and S.C.J.; visualization, A.S.; supervision, S.C.J.; project administration, S.C.J. All authors have read and agreed to the published version of the manuscript.

Funding: This research received no external funding.

Data Availability Statement: This study does not utilize any external or commercial datasets. The samples and test data are available upon request.

Acknowledgments: The first author acknowledges the research scholarship received from Nanyang Technological University, Singapore. The authors are grateful for the support and resources provided by the School of Mechanical and Aerospace Engineering at Nanyang Technological University, Singapore. The authors also extend their appreciation to Dow Chemical Pacific (Singapore) Private Limited for providing the Paraloid EXL-2314 CSPs. Furthermore, the authors wish to thank Chia Hwee Lang, Akash Singaram, Justin, and Selvakumaran for their assistance in testing.

Conflicts of Interest: The authors declare no conflicts of interest.

References

1. Sharma, A.; Joshi, S.C. Fiber-reinforced polyurethane matrix composites for engineering applications. In *Polyurethanes: Preparation, Properties, and Applications Volume 1: Fundamentals*; ACS Publications: Washington, DC, USA, 2023; pp. 101–118. [CrossRef]
2. Yao, S.-S.; Jin, F.-L.; Rhee, K.Y.; Hui, D.; Park, S.-J. Recent advances in carbon-fiber-reinforced thermoplastic composites: A review. *Compos. Part B Eng.* **2018**, *142*, 241–250. [CrossRef]
3. Nguyen-Tran, H.-D.; Hoang, V.-T.; Do, V.-T.; Chun, D.-M.; Yum, Y.-J. Effect of multiwalled carbon nanotubes on the mechanical properties of carbon fiber-reinforced polyamide-6/polypropylene composites for lightweight automotive parts. *Materials* **2018**, *11*, 429. [CrossRef] [PubMed]
4. Sang, L.; Wang, Y.; Wang, C.; Peng, X.; Hou, W.; Tong, L. Moisture diffusion and damage characteristics of carbon fabric reinforced polyamide 6 laminates under hydrothermal aging. *Compos. Part A Appl. Sci. Manuf.* **2019**, *123*, 242–252. [CrossRef]
5. Ma, Y.; Ueda, M.; Yokozeki, T.; Sugahara, T.; Yang, Y.; Hamada, H. A comparative study of the mechanical properties and failure behavior of carbon fiber/epoxy and carbon fiber/polyamide 6 unidirectional composites. *Compos. Struct.* **2017**, *160*, 89–99. [CrossRef]
6. Alshammari, B.A.; Alsuhybani, M.S.; Almushaikeh, A.M.; Alotaibi, B.M.; Alenad, A.M.; Alqahtani, N.B.; Alharbi, A.G. Comprehensive review of the properties and modifications of carbon fiber-reinforced thermoplastic composites. *Polymers* **2021**, *13*, 2474. [CrossRef]
7. Sharma, A.; Joshi, S.C. Enhancement in Fatigue Performance of FRP composites with various fillers: A review. *Compos. Struct.* **2023**, *309*, 116724. [CrossRef]
8. Huang, T.; Bobyr, M. A review of delamination damage of composite materials. *J. Compos. Sci.* **2023**, *7*, 468. [CrossRef]
9. Borrego, L.; Costa, J.; Ferreira, J.; Silva, H. Fatigue behaviour of glass fibre reinforced epoxy composites enhanced with nanoparticles. *Compos. Part B Eng.* **2014**, *62*, 65–72. [CrossRef]
10. Chen, H.; Wang, J.; Ni, A.; Ding, A.; Li, S.; Han, X. Effect of nano-OMMTs on mode I and mode II fracture toughness of continuous glass fibre reinforced polypropylene composites. *Compos. Struct.* **2019**, *208*, 498–506. [CrossRef]
11. Damodaran, V.; Castellanos, A.; Milostan, M.; Prabhakar, P. Improving the Mode-II interlaminar fracture toughness of polymeric matrix composites through additive manufacturing. *Mater. Des.* **2018**, *157*, 60–73. [CrossRef]
12. Bhudolia, S.K.; Gohel, G.; Joshi, S.C.; Leong, K.F. Manufacturing optimization and experimental investigation of ex-situ core-shell particles toughened carbon/elium® thermoplastic composites. *Fibers Polym.* **2021**, *22*, 1693–1703. [CrossRef]
13. Chen, Q.; Boisse, P.; Park, C.H.; Saouab, A.; Bréard, J. Intra/inter-ply shear behaviors of continuous fiber reinforced thermoplastic composites in thermoforming processes. *Compos. Struct.* **2011**, *93*, 1692–1703. [CrossRef]
14. Arquier, R.; Sabatier, H.; Iliopoulos, I.; Régnier, G.; Miquelard-Garnier, G. Role of the inter-ply microstructure in the consolidation quality of high-performance thermoplastic composites. *Polym. Compos.* **2024**, *45*, 1218–1227. [CrossRef]
15. Yan, C.; Zhu, Y.; Liu, D.; Xu, H.; Chen, G.; Chen, M.; Cai, G. Improving interfacial adhesion and mechanical properties of carbon fiber reinforced polyamide 6 composites with environment-friendly water-based sizing agent. *Compos. Part B Eng.* **2023**, *258*, 110675. [CrossRef]
16. Gokce, E.C.; Gungor, M.; Kilic, A.; Acma, M.E. Improving the Interfacial Adhesion of Long Carbon Fiber-Reinforced Polyamide 6 Composites by Electrochemical Oxidation and Polyethylenimine-Carboxymethyl Cellulose Grafting. *ACS Omega* **2024**, *9*, 32547–32556. [CrossRef]
17. Yan, F.; Yan, T.; Wang, G.; Li, G.; Dai, S.; Ao, Y.; Duan, J.; Liu, L. A novel thermoplastic water-soluble sizing agent for the interfacial enhancement of carbon fiber/polyether ether ketone composites. *Compos. Part B Eng.* **2024**, *272*, 111205. [CrossRef]

18. Huang, C.; Zhang, P.; Li, B.; Sun, M.; Liu, H.; Sun, J.; Zhao, Y.; Bao, J. A Water-Soluble Thermoplastic Polyamide Acid Sizing Agents for Enhancing Interfacial Properties of Carbon Fibre Reinforced Polyimide Composites. *Materials* **2024**, *17*, 2559. [CrossRef] [PubMed]
19. Jian, L. Effect of sizing agent on interfacial properties of carbon fiber-reinforced PMMA composite. *Compos. Adv. Mater.* **2021**, *30*, 2633366X20978657. [CrossRef]
20. Liu, H.; Zhao, Y.; Li, N.; Li, S.; Li, X.; Liu, Z.; Cheng, S.; Wang, K.; Du, S. Effect of polyetherimide sizing on surface properties of carbon fiber and interfacial strength of carbon fiber/polyetheretherketone composites. *Polym. Compos.* **2021**, *42*, 931–943. [CrossRef]
21. Nassehi, V.; Dhillon, J.; Mascia, L. Finite element simulation of the micromechanics of interlayered polymer/fibre composites: A study of the interactions between the reinforcing phases. *Compos. Sci. Technol.* **1993**, *47*, 349–358. [CrossRef]
22. Nassehi, V.; Kinsella, M.; Mascia, L. Finite element modelling of the stress distribution in polymer composites with coated fibre interlayers. *J. Compos. Mater.* **1993**, *27*, 195–214. [CrossRef]
23. Zheng, H.; Zhang, W.; Li, B.; Zhu, J.; Wang, C.; Song, G.; Wu, G.; Yang, X.; Huang, Y.; Ma, L. Recent advances of interphases in carbon fiber-reinforced polymer composites: A review. *Compos. Part B Eng.* **2022**, *233*, 109639. [CrossRef]
24. Qiu, B.; Li, M.; Zhang, X.; Chen, Y.; Zhou, S.; Liang, M.; Zou, H. Carboxymethyl cellulose sizing repairs carbon fiber surface defects in epoxy composites. *Mater. Chem. Phys.* **2021**, *258*, 123677. [CrossRef]
25. Han, W.; Zhang, H.-P.; Tavakoli, J.; Campbell, J.; Tang, Y. Polydopamine as sizing on carbon fiber surfaces for enhancement of epoxy laminated composites. *Compos. Part A Appl. Sci. Manuf.* **2018**, *107*, 626–632. [CrossRef]
26. Chen, S.; Cao, Y.; Feng, J. Polydopamine as an efficient and robust platform to functionalize carbon fiber for high-performance polymer composites. *ACS Appl. Mater. Interfaces* **2014**, *6*, 349–356. [CrossRef]
27. Yang, X.; Du, H.; Li, S.; Wang, Z.; Shao, L. Codepositing mussel-inspired nanohybrids onto one-dimensional fibers under "green" conditions for significantly enhanced surface/interfacial properties. *ACS Sustain. Chem. Eng.* **2018**, *6*, 4412–4420. [CrossRef]
28. Liu, L.; Ying, G.; Hu, C.; Zhang, K.; Ma, F.; Su, L.; Zhang, C.; Wang, C. Functionalization with MXene (Ti_3C_2) enhances the wettability and shear strength of carbon fiber-epoxy composites. *ACS Appl. Nano Mater.* **2019**, *2*, 5553–5562. [CrossRef]
29. Periasamy, K.; Kandare, E.; Das, R.; Darouie, M.; Khatibi, A.A. Interfacial engineering methods in thermoplastic composites: An overview. *Polymers* **2023**, *15*, 415. [CrossRef]
30. Jin, Z.; Han, Z.; Chang, C.; Sun, S.; Fu, H. Review of methods for enhancing interlaminar mechanical properties of fiber-reinforced thermoplastic composites: Interfacial modification, nano-filling and forming technology. *Compos. Sci. Technol.* **2022**, *228*, 109660. [CrossRef]
31. Yavuz, Z.; Öz, Y.; Ece, R.E.; Öztürk, F. Investigation of sizing materials for carbon fiber reinforced thermoplastic composites. *J. Thermoplast. Compos. Mater.* **2024**, 08927057241284794. [CrossRef]
32. Shen, Z.; Bateman, S.; Wu, D.Y.; McMahon, P.; Dell'Olio, M.; Gotama, J. The effects of carbon nanotubes on mechanical and thermal properties of woven glass fibre reinforced polyamide-6 nanocomposites. *Compos. Sci. Technol.* **2009**, *69*, 239–244. [CrossRef]
33. Chen, J.; Zhang, T.; Wang, K.; Zhao, Y. Multiscale enhancement behavior of nano-silica modified CF/PEEK composites prepared by wet powder impregnation. *Polym. Compos.* **2019**, *40*, 1187–1197. [CrossRef]
34. Qiao, L.; Zhu, K.; Tan, H.; Yan, X.; Zheng, L.; Dong, S. Effect of carbon nanotubes on the electrical, thermal, mechanical properties and crystallization behavior of continuous carbon fiber reinforced polyether-ether-ketone composites. *Mater. Res. Express* **2021**, *8*, 045312. [CrossRef]
35. Su, Y.; Zhang, S.; Zhang, X.; Zhao, Z.; Jing, D. Preparation and properties of carbon nanotubes/carbon fiber/poly (ether ether ketone) multiscale composites. *Compos. Part A Appl. Sci. Manuf.* **2018**, *108*, 89–98. [CrossRef]
36. Bhudolia, S.K.; Gohel, G.; Joshi, S.C.; Leong, K.F. Quasi-static indentation response of core-shell particle reinforced novel nccf/elium® composites at different feed rates. *Compos. Commun.* **2020**, *21*, 100383. [CrossRef]
37. Santos, L.F.; Ribeiro, B.; Hein, L.R.; Alderliesten, R.; Zarouchas, D.; Botelho, E.C.; Costa, M.L. The effect of temperature on fatigue strength of poly (ether-imide)/multiwalled carbon nanotube/carbon fibers composites for aeronautical application. *J. Appl. Polym. Sci.* **2020**, *137*, 49160. [CrossRef]
38. Song, J.-p.; Zhao, Y.; Li, X.-k.; Xiong, S.; Li, S.; Wang, K. Increasing the toughness while reducing the viscosity of carbon nano-tube/polyether imide/polyether ether ketone nanocomposites. *New Carbon Mater.* **2024**, *39*, 715–728. [CrossRef]
39. Di Boon, Y.; Joshi, S.C. A review of methods for improving interlaminar interfaces and fracture toughness of laminated composites. *Mater. Today Commun.* **2020**, *22*, 100830. [CrossRef]
40. Ali, M.; Joshi, S.C. Impact damage resistance of CFRP prepreg laminates with dispersed CSP particles into ply interfaces. *Int. J. Damage Mech.* **2012**, *21*, 1106–1127. [CrossRef]
41. Bhudolia, S.K.; Gohel, G.; Joshi, S.C.; Leong, K.F. Vibration damping and dynamic mechanical attributes of core-shell particles modified glass epoxy prepregs cured using microwave irradiations. *Compos. Commun.* **2020**, *21*, 100412. [CrossRef]
42. Sharma, A.; Joshi, S.C. Effect of in-situ activated core-shell particles on fatigue behavior of carbon fiber reinforced thermoplastic composites. *Compos. Sci. Technol.* **2024**, *253*, 110654. [CrossRef]
43. Phong, N.T.; Gabr, M.H.; Anh, L.H.; Duc, V.M.; Betti, A.; Okubo, K.; Chuong, B.; Fujii, T. Improved fracture toughness and fatigue life of carbon fiber reinforced epoxy composite due to incorporation of rubber nanoparticles. *J. Mater. Sci.* **2013**, *48*, 6039–6047. [CrossRef]

44. Ali, M.M.; Joshi, S.C. Optimal layup schemes with selective dispersion of core/shell microparticles in ply interfaces of glass/epoxy composite laminates for low velocity impact. *J. Phys. Conf. Ser.* **2019**, *1355*, 012042.
45. Ngah, S.A.; Taylor, A.C. Toughening performance of glass fibre composites with core–shell rubber and silica nanoparticle modified matrices. *Compos. Part A Appl. Sci. Manuf.* **2016**, *80*, 292–303. [CrossRef]
46. *ASTM D7264*; Standard Test Method for Flexural Properties of Polymer Matrix Composite Materials. ASTM International, American Society for Testing and Materials: West Conshohocken, PA, USA, 2015.
47. *ASTM D2344*; Standard Test Method for Short-Beam Strength of Polymer Matrix Composite Materials and Their Laminates. ASTM International, American Society for Testing and Materials: West Conshohocken, PA, USA, 2006.
48. *ASTM D695*; Standard Test Method for Compressive Properties of Rigid Plastics. ASTM International, American Society for Testing and Materials: West Conshohocken, PA, USA, 2010.
49. Ignatius, W. *Fiber Fraction in Woven Structures*; Arcada University of Applied Sciences: Helsinki, Finland, 2018.
50. *ASTM D2734-09*; Standard Test Methods for Void Content of Reinforced Plastics. ASTM International, American Society for Testing and Materials: West Conshohocken, PA, USA, 2009.
51. Mehdikhani, M.; Gorbatikh, L.; Verpoest, I.; Lomov, S.V. Voids in fiber-reinforced polymer composites: A review on their formation, characteristics, and effects on mechanical performance. *J. Compos. Mater.* **2019**, *53*, 1579–1669. [CrossRef]
52. Ma, Y.; Yokozeki, T.; Ueda, M.; Sugahara, T.; Yang, Y.; Hamada, H. Effect of polyurethane dispersion as surface treatment for carbon fabrics on mechanical properties of carbon/Nylon composites. *Compos. Sci. Technol.* **2017**, *151*, 268–281. [CrossRef]
53. Zhao, D.; Ma, Y.; Yang, Y. Flexural damage behavior of CF/PA6 plain woven laminates with different layers. *Compos. Part B Eng.* **2019**, *162*, 631–642. [CrossRef]